Precise Diagnosis of Tumor Cells and Hemocyte via Ultrasensitive, Stable, Selective Cuprous Oxide Composite SERS Bioprobe Assisted with High Efficiency Separation Microfluidic Chip

Yujiao Xie[a,b#], Lei Xu[a,b#], Jiahao Zhang[a,b#], Chenguang Zhang[a,b#], Yue Hu[a,b], Zhouxu Zhang[a,b], Guoxin Chen[ab], Shuyan Qi[ab], Xiawei Xu[ab], Jing Wang[a,b], Wenzhi Ren[a,b], Jie Lin[*ab], Aiguo Wu[*ab]

[a] Laboratory of Advanced Theranostic Materials and Technology, Ningbo Institute of Materials Technology and Engineering, Zhejiang International Cooperation Base of Biomedical Materials Technology and Application, Ningbo Institute of Materials Technology and Engineering, Chinese Academy of Sciences, Ningbo, 315201, China
[b] Ningbo Cixi institute of Biomedical Engineering, Ningbo, 315201, China

[#]These authors contributed equally.

Corresponding Authors:

Prof. Aiguo Wu, Ningbo Key Laboratory of Biomedical Imaging Probe Materials and Technology, Zhejiang International Cooperation Base of Biomedical Materials Technology and Application, Chinese Academy of Sciences (CAS) Key Laboratory of Magnetic Materials and Devices, Ningbo Cixi Institute of Biomedical Engineering, Zhejiang Engineering Research Center for Biomedical Materials, Ningbo Institute of Materials Technology and Engineering, Chinese Academy of Sciences, Ningbo, 315201, China; aiguo@nimte.ac.cn

Prof. Jie Lin, Ningbo Key Laboratory of Biomedical Imaging Probe Materials and Technology, Zhejiang International Cooperation Base of Biomedical Materials Technology and Application, Chinese Academy of Sciences (CAS) Key Laboratory of Magnetic Materials and Devices, Ningbo Cixi Institute of Biomedical Engineering, Zhejiang Engineering Research Center for Biomedical Materials, Ningbo Institute of Materials Technology and Engineering, Chinese Academy of Sciences, Ningbo, 315201, China; linjie@nimte.ac.cn

1. Materials

Polyvinylpyrrolidone (PVP, Mw ≈ 1300000), $CuCl_2 \cdot 2H_2O$, ascorbic acid ($C_6H_8O_6$) and methylene blue methylene blue (MB) were purchased by Macklin Biochemical Technology Co., Ltd. (Shanghai, China). Sodium borohydride ($NaBH_4$) and silver nitrate ($AgNO_3$) were acquired from China National Pharmaceutical Group Co., Ltd. Alizarin red (AR), crystal violet (CV), 4 mercaptopyridine (4MPY), Na_2SO_4 and NaOH were procured from Aladdin Biochemical Technology Co., Ltd. (Shanghai, China). Sodium citrate ($C_6H_5Na_3O_7$) was supplied by Titan Scientific Co., Ltd. (Shanghai, China). Tween 20 was purchased by Sigma-Aldrich. Fluorescent polystyrene microspheres were purchased by Yuyuan Biotech (Shanghai, China) and BaseLine ChromTech Research Centre (Tianjin, China). Inertial microfluidic chips were fabricated by Suzhou Zhongxin Qiheng Chip Technology Co., Ltd. Fluorescently labeled U251 cell line was purchased by OriCell® (Guangzhou, China), T24 cell line was provided by Ruyao Biotechnology (Ningbo, China), PANC02 cell line was supported by Cancer Research Institute, Zhejiang University (Hangzhou, China). Dulbecco's modified Eagle medium (DMEM), fetal bovine serum (FBS), and trypsin-ethylenediaminetetraacetic acid were obtained from Gibco Life Technologies. Sodium citrate anticoagulant rabbit blood was provided by SenBeiJia Biological Technology Co., Ltd. Deionized water was prepared with Milli-Q® Direct System. All other chemical reagents were used without further purifications.

2. Physical characterization of flower-like Cu_2O, Cu_2O@Ag

The morphology of Cu_2O and Cu_2O@Ag were analyzed using transmission electron microscope (Talos, HITACHI) and scanning electron microscope (SEM, HITACHI). The selected area electron diffraction image and high-resolution lattice pattern were recorded by JEOL F200. The absorption characteristics were measured using a T10 CS UV−vis spectrophotometer from Beijing Purkinje General Instrument CO., Ltd. The powder's X-ray diffraction (XRD) was analyzed utilizing the BRUKER D8 ADVANCE DAVINCI diffractometer with Cu Kα radiation (λ = 1.54056 Å). X-ray photoelectron spectroscopy (XPS, Axis Ultra Axis Ultra DLD, Shimadzu) was used to analyze the composition of element, band structure and chemical bonding. Photoluminescence (PL) was measured by confocal Raman microscope (inVia Reflex, Renishaw) at 532 nm laser source. The confocal Raman microscope (Labram Odyssey, Horiba) equipped with 473 nm, 532 nm, 633 nm, and 785 nm laser sources was used to compare Raman intensity under different laser wavelength. Steady state and transient state fluorescence spectrometer (Fluorolog-QM, Horiba) was used to measure fluorescence lifetime. Mott–Schottky and photocurrent curves were recorded by electrochemical workstation (CHI760E, CHINSTRUMENT) connected to a cell containing three electrodes (a gold working electrode, Ag/AgCl reference electrode, graphite counter electrode) and sodium sulfate (Na_2SO_4, 0.5 M pH 7.0) aqueous electrolyte. Diffuse reflection profiles were recorded by UV/Vis/NIR Spectrophotometer (Lambda 950, Perkin-Elmer). Spherical aberration corrected transmission electron microscope (AC-TEM, Spectra300, ThermoFisher) was used to observe surface defect.

3. Morphology characterization of flower-like Cu_2O

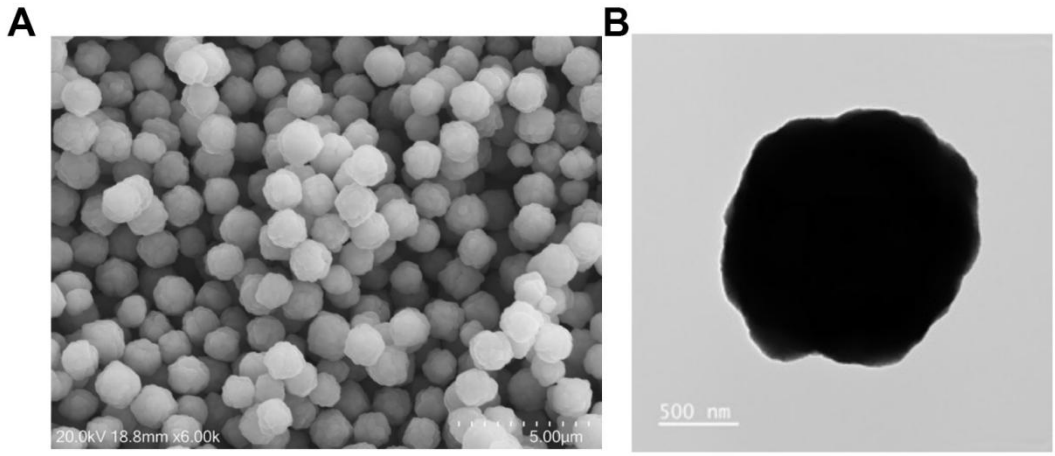

Figure S1. Wide field of SEM (A) and TEM (B) images of flower-like Cu_2O.

4. Lattice fringe and selected area electron diffraction images of flower-like Cu_2O

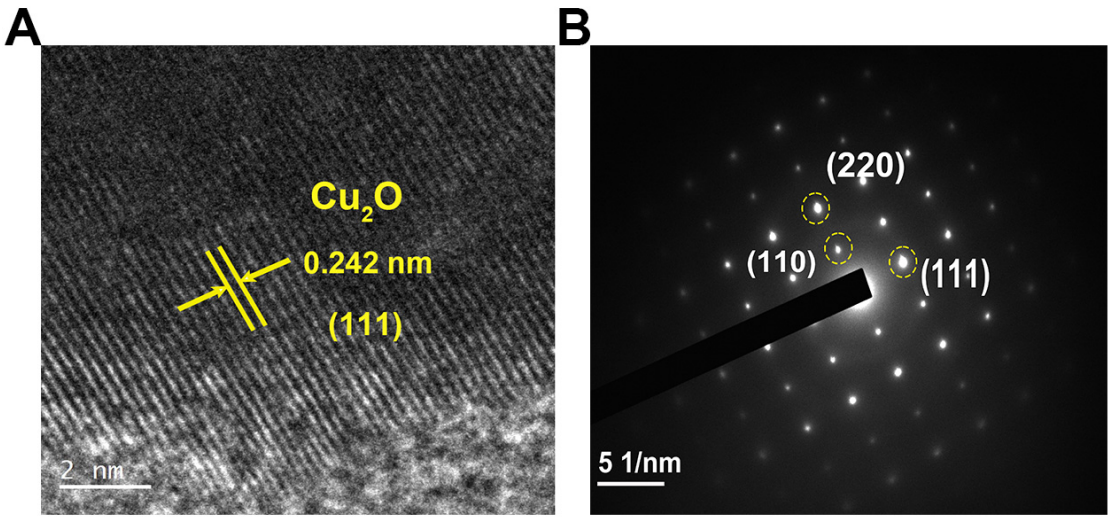

Figure S2. Lattice fringe pattern (A) and selected area electron diffraction image (B) of flower-like Cu_2O under HRTEM.

5. Element scanning images of flower-like Cu_2O

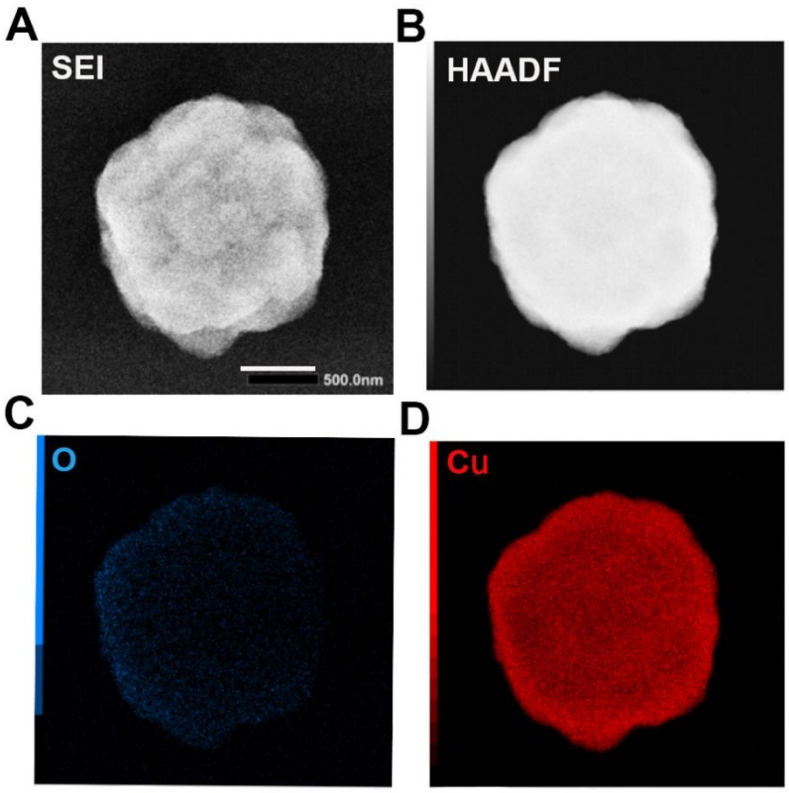

Figure S3. Element scanning images of flower-like Cu_2O.

6. Wide field of SEM image of Cu_2O@Ag

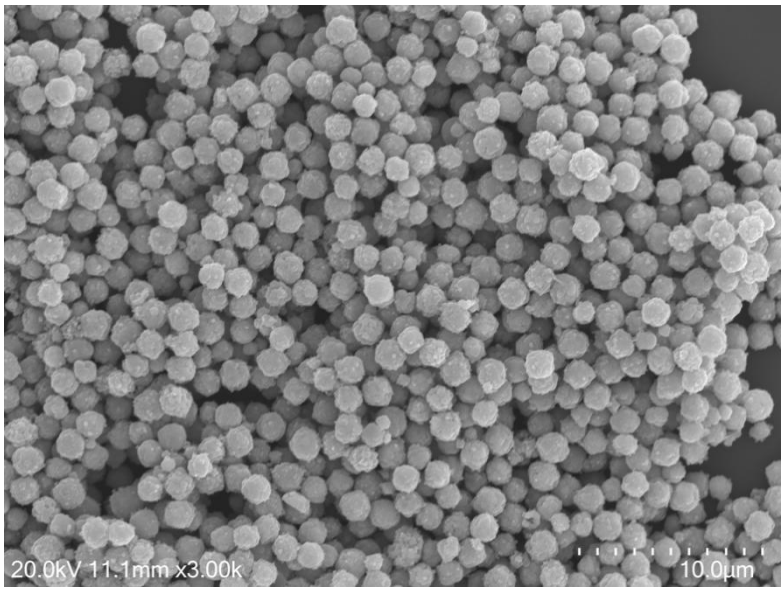

Figure S4. Wide field of SEM image of Cu_2O@Ag.

7. High resolution XPS spectra of flower-like Cu_2O and Cu_2O@Ag

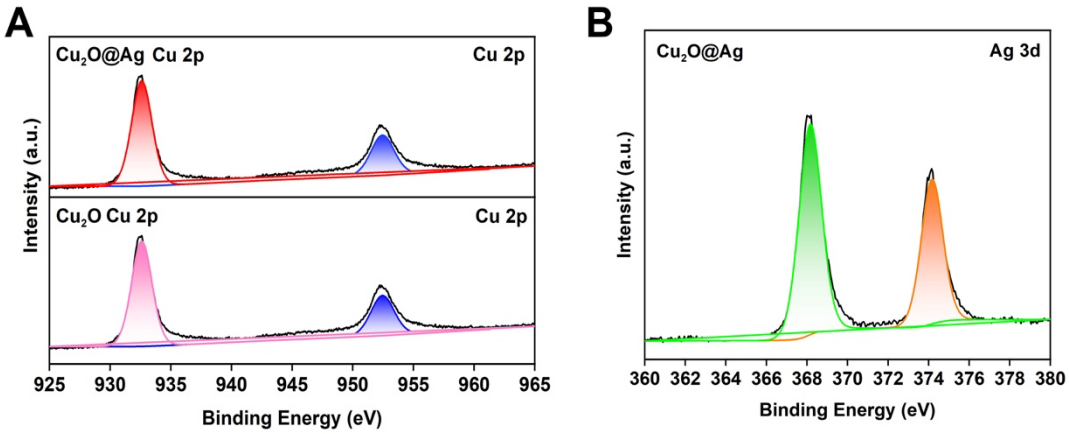

Figure S5. High resolution XPS spectra of Cu 2p of flower-like Cu_2O and Cu_2O@Ag (A) and Ag 3d spectrum of Cu_2O@Ag (B).

8. Storage stability of flower-like Cu_2O@Ag

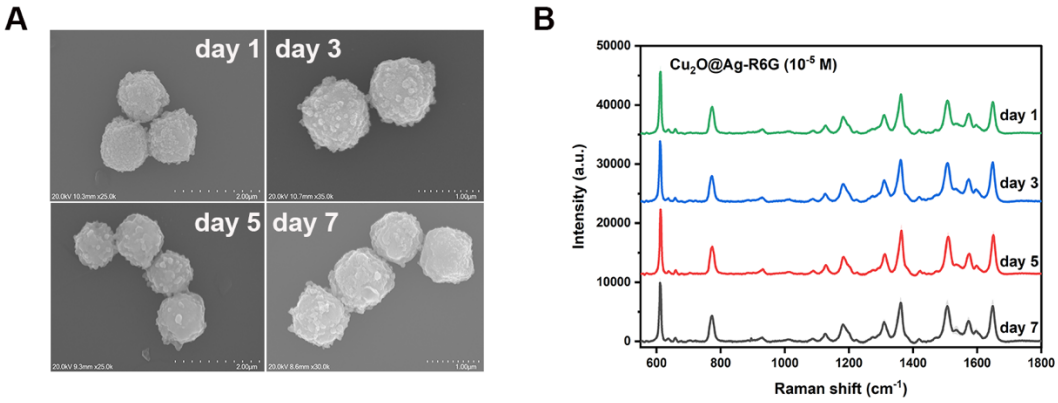

Figure S6. The SEM images of flower Cu_2O@Ag and SERS spectra of Cu_2O@Ag-R6G (10^{-5} M) within 7 days.

9. Electromagnetic field simulation of Ag, flower-like Cu_2O and Cu_2O@Ag under excitation at 514 nm

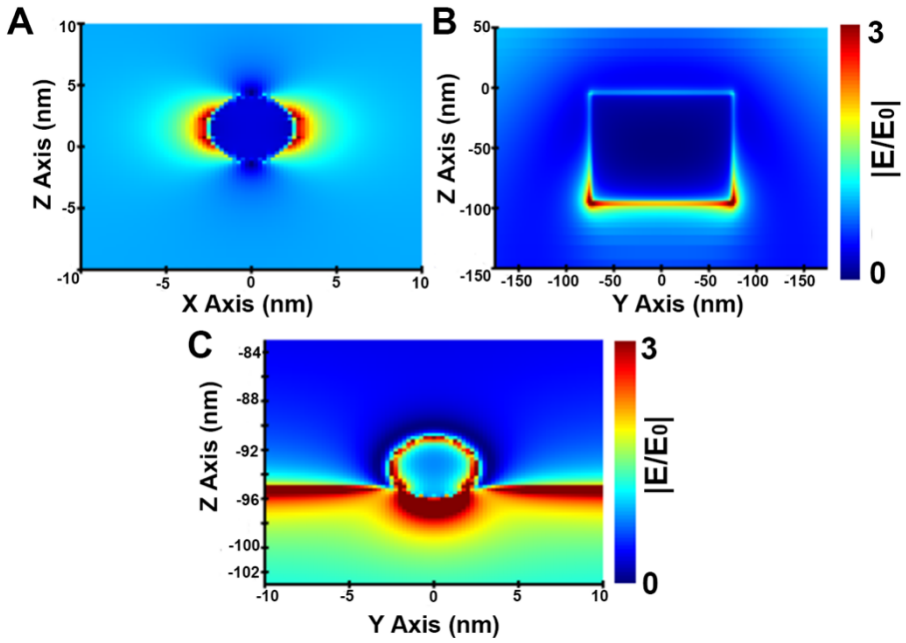

Figure S7. Electromagnetic field simulation of Ag (A), flower-like Cu_2O (B) and Cu_2O@Ag (C) under excitation at 514 nm.

10. Fluorescence spectra of MB solution, Cu_2O-MB and Cu_2O@Ag-MB

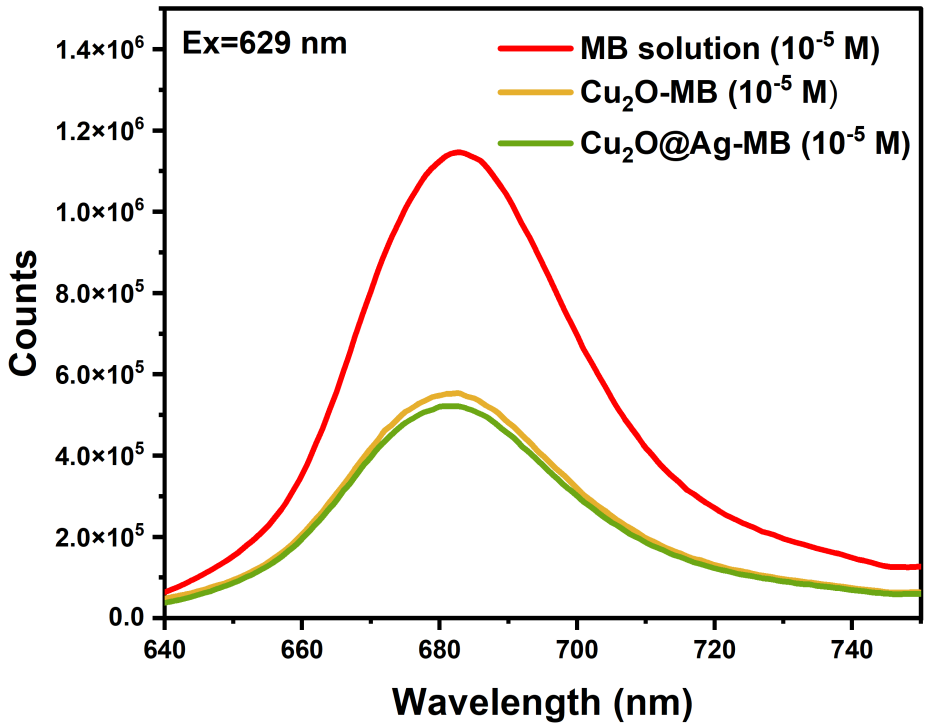

Figure S8. Fluorescence spectra of MB solution (10^{-5} M), Cu_2O-MB (10^{-5} M) and Cu_2O@Ag-MB (10^{-5} M).

11. Valence band of flower-like Cu_2O and Cu_2O@Ag

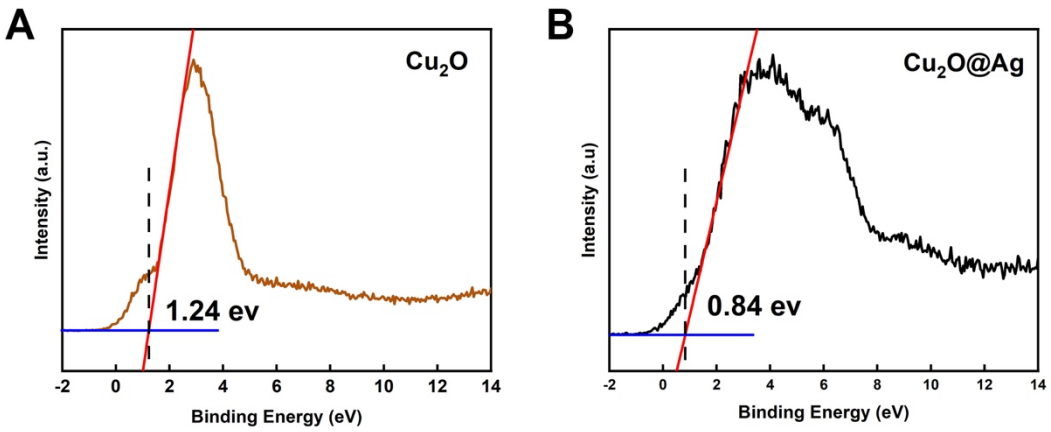

Figure S9. Valence band of flower-like Cu_2O and Cu_2O@Ag.

12. Mott–Schottky plots of flower-like Cu_2O and Cu_2O@Ag

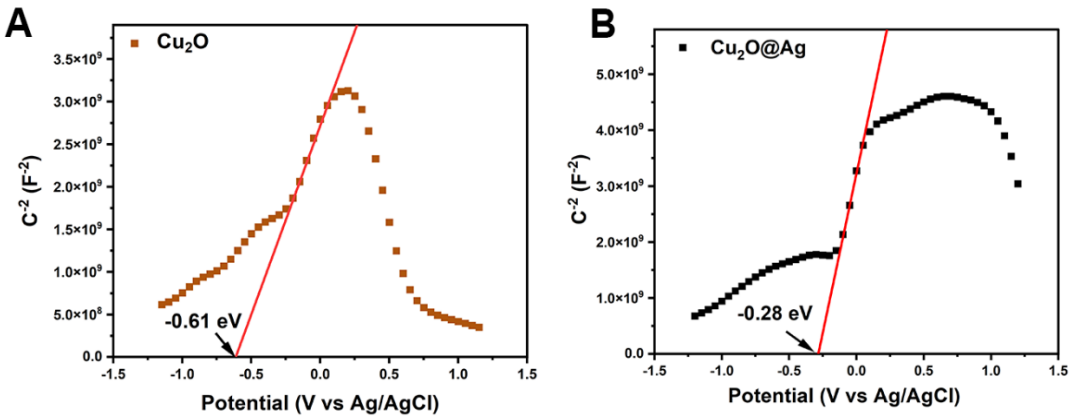

Figure S10. Mott–Schottky plots of flower-like Cu_2O (A) and Cu_2O@Ag (B).

13. Band gap of flower-like Cu_2O and Cu_2O@Ag

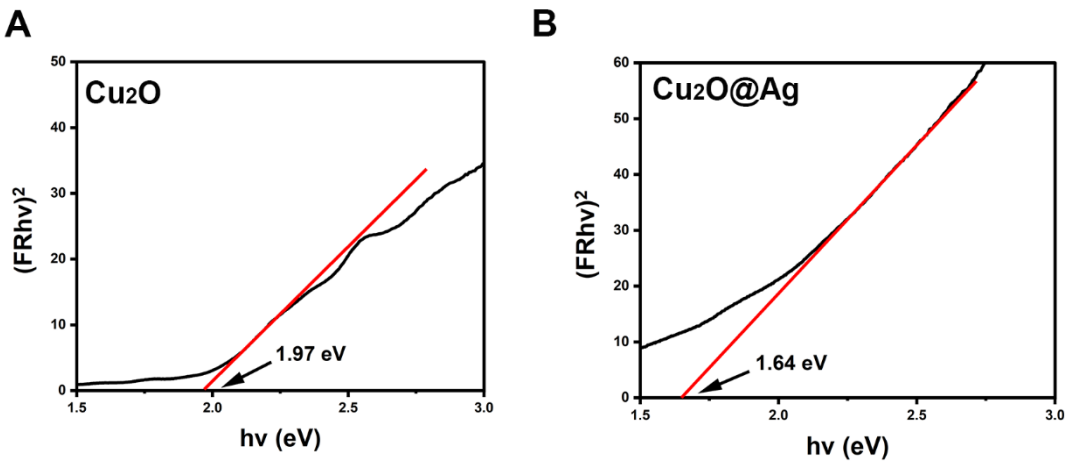

Figure S11. Band gap of flower-like Cu_2O (A) and Cu_2O@Ag (B).

14. Comparison of energy bands between flower-like Cu_2O and Cu_2O@Ag

Table S1. Table of energy bands of flower-like Cu_2O and Cu_2O@Ag

	CB (eV)	**VB (eV)**	**Ef (eV)**	**Ef-VB (eV)**	**CB-VB (eV)**
Cu_2O	-3.77	-5.74	-4.5	1.24	1.97
Cu_2O@Ag	-4	-5.64	-4.8	0.84	1.64

15. Morphology characterization of octahedral Cu_2O

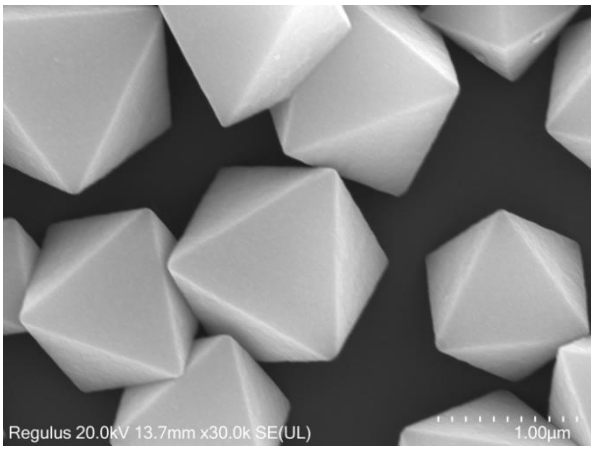

Figure S12. SEM image of octahedral Cu_2O.

16. Bright field images of inertial microfluidic chip

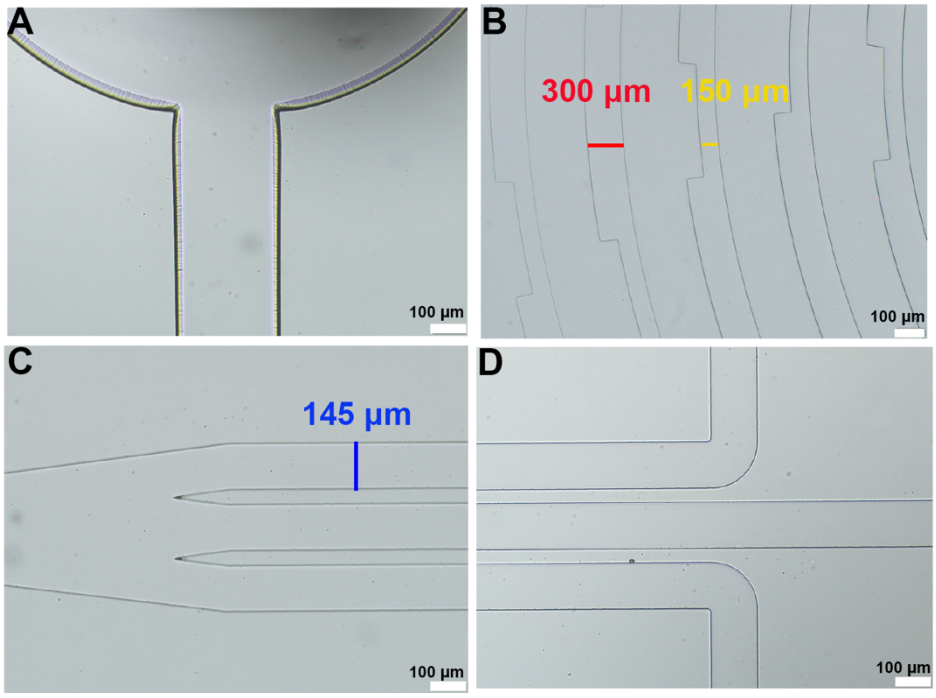

Figure S13. Bright field images of inertial microfluidic chip. Inlet (A), channel (B), and outlets (C-D) of microfluidic chip.

17. Movement trajectories of fluorescent microspheres at microfluidic channels and furcation

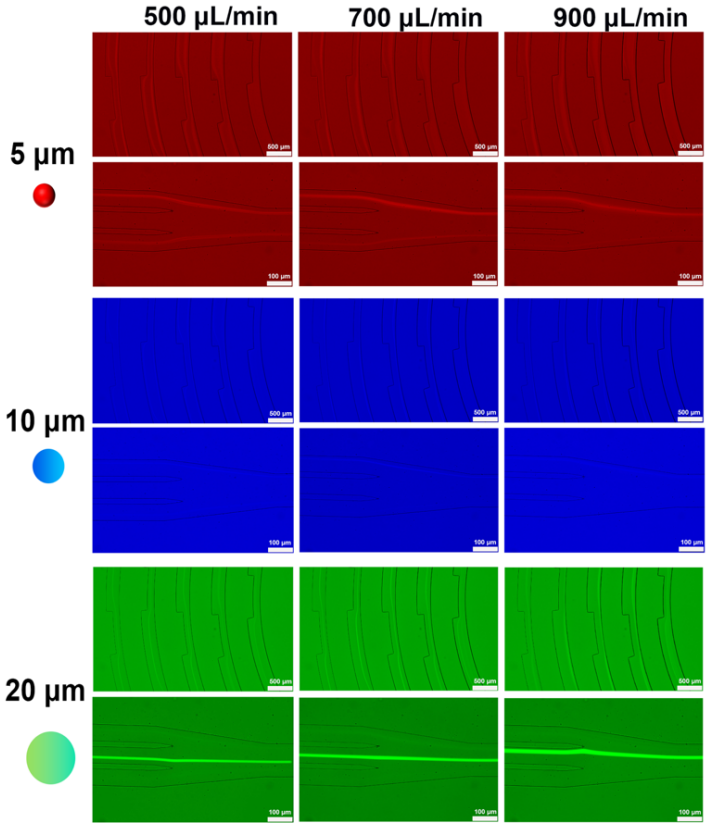

Figure S14. Movement trajectories of 5 μm, 10 μm and 20 μm fluorescent microspheres at microfluidic channels and furcation.

18. Bright field and fluorescence images of fluorescently labelled T24, U251 and Panc02 cells collected from outlets of microfluidic chip

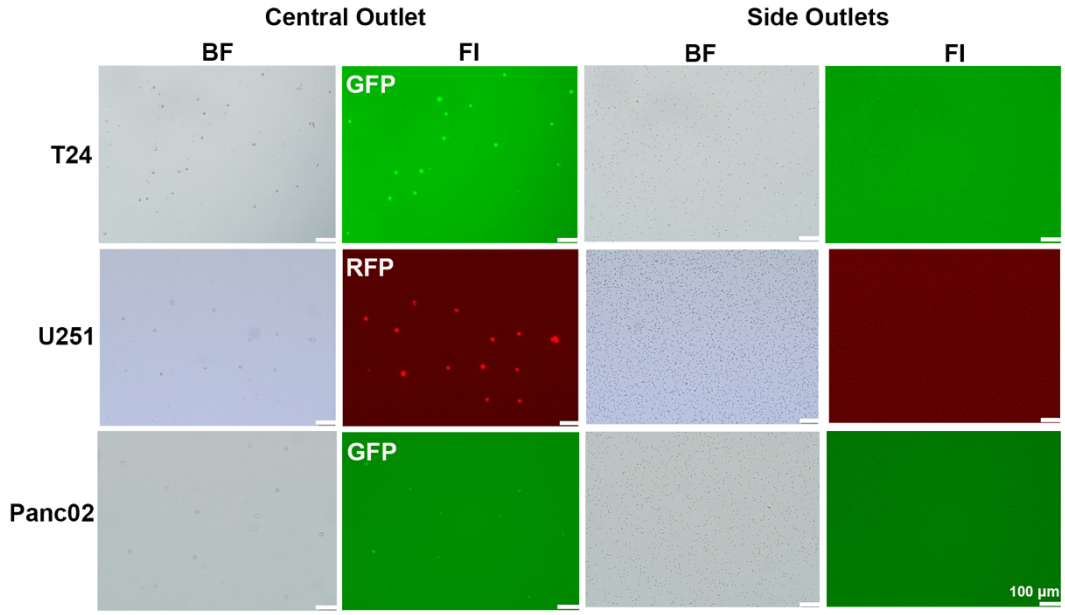

Figure S15. Bright field and fluorescence images of fluorescently labelled T24, U251 and Panc02 cells collected from outlets of microfluidic chip.

19. Comparison of the mean fluorescence intensity of cancer cells in blood sample with serum and serum free after being separated via microfluidic chip

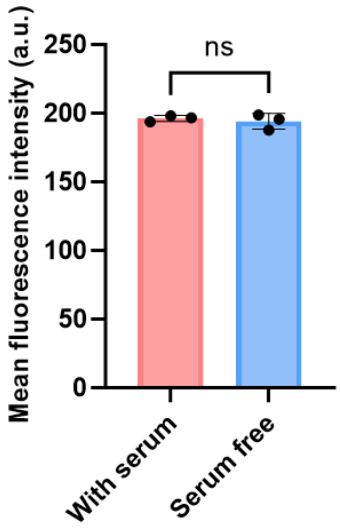

Figure S16. The mean fluorescence intensity of cancer cells in blood sample with serum and serum free after being separated via microfluidic chip.

20. Size distribution of T24, U251 and Panc02 cells collected from central outlet of microfluidic chip

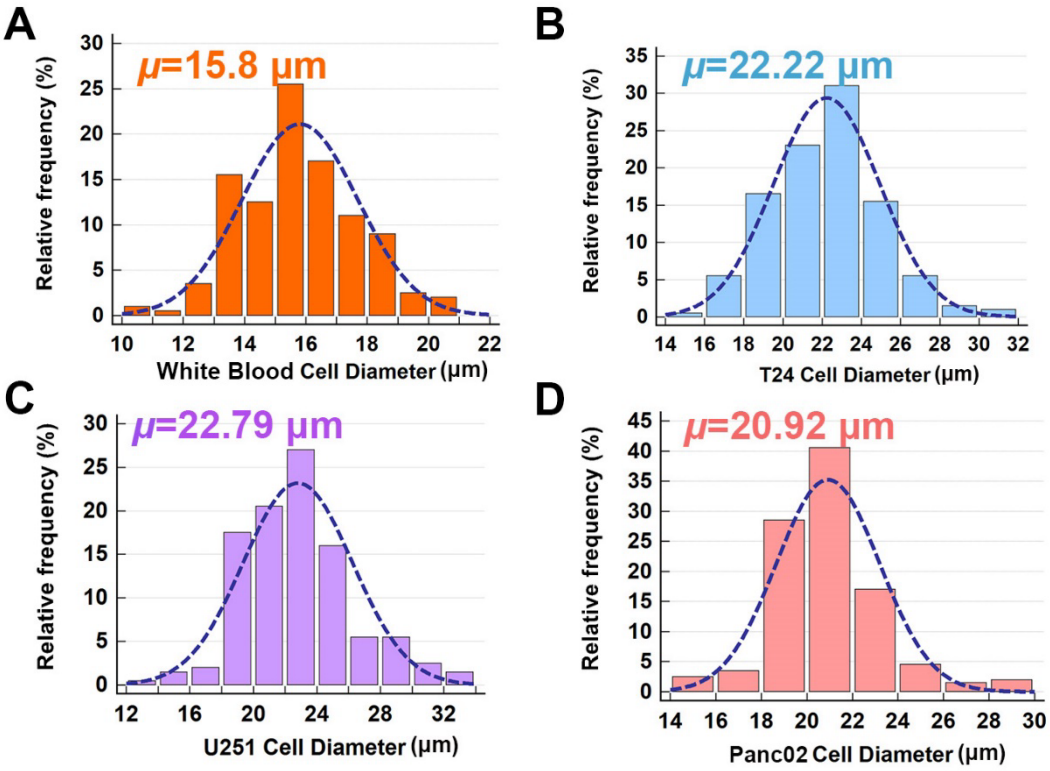

Figure S17. Size distribution of WBC, T24, U251 and Panc02 cells collected from central outlet of microfluidic chip.

21. Average label-free SERS spectra of T24, U251 and Panc02 cells collected from central outlet of microfluidic chip

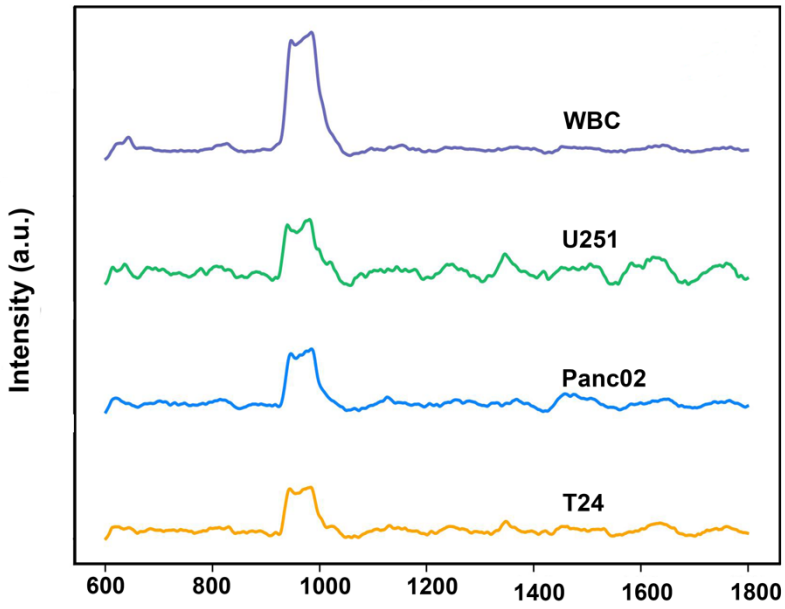

Figure S18. Average label-free SERS spectra of T24, U251 and Panc02 cells collected from central outlet of microfluidic chip.